

---

# FEDERATED BAYESIAN DEEP LEARNING: THE APPLICATION OF STATISTICAL AGGREGATION METHODS TO BAYESIAN MODELS

---

A PREPRINT

**John Fischer**

Department of Computer Science  
Naval Postgraduate School  
Monterey, CA 93954  
john.fischer@nps.edu

**Marko Orescanin**

Department of Computer Science  
Naval Postgraduate School  
Monterey, CA 93954  
marko.orescanin@nps.edu

**Justin Loomis**

Department of Computer Science  
Naval Postgraduate School  
Monterey, CA 93954

**Patrick McClure**

Department of Computer Science  
Naval Postgraduate School  
Monterey, CA 93954

March 22, 2024

## ABSTRACT

Federated learning (FL) is an approach to training machine learning models that takes advantage of multiple distributed datasets while maintaining data privacy and reducing communication costs associated with sharing local datasets. Aggregation strategies have been developed to pool or fuse the weights and biases of distributed deterministic models; however, modern deterministic deep learning (DL) models are often poorly calibrated and lack the ability to communicate a measure of epistemic uncertainty in prediction, which is desirable for remote sensing platforms and safety-critical applications. Conversely, Bayesian DL models are often well calibrated and capable of quantifying and communicating a measure of epistemic uncertainty along with a competitive prediction accuracy. Unfortunately, because the weights and biases in Bayesian DL models are defined by a probability distribution, simple application of the aggregation methods associated with FL schemes for deterministic models is either impossible or results in sub-optimal performance. In this work, we use independent and identically distributed (IID) and non-IID partitions of the CIFAR-10 dataset and a fully variational ResNet-20 architecture to analyze six different aggregation strategies for Bayesian DL models. Additionally, we analyze the traditional federated averaging approach applied to an approximate Bayesian Monte Carlo dropout model as a lightweight alternative to more complex variational inference methods in FL. We show that aggregation strategy is a key hyperparameter in the design of a Bayesian FL system with downstream effects on accuracy, calibration, uncertainty quantification, training stability, and client compute requirements.

**Keywords** Bayesian deep learning · federated learning · Monte Carlo dropout · uncertainty decomposition · uncertainty quantification · variational inference

## 1 Introduction

### 1.1 Motivation

Remote sensors are ubiquitous in the world today. This is due to the continual advancement in hardware technology, which supports their deployment in ever-shrinking, affordable devices. The mass deployment of remote sensors has resulted in an explosion in the amount of data collected in support of various research groups, corporations, and government entities [1]. The overwhelming task of analyzing this data has resulted in a desire to automate or to augment

data analysis using deep learning (DL) techniques. In many remote sensing applications, the cost of collecting, labeling, communicating, and storing local data may be acceptable; however, when deploying sensors all over the world, these costs can breach the threshold of acceptability. In other applications, the transfer and storage of user data raises data privacy concerns and regulations, such as the General Data Protection Regulation (GDPR) [2], and imposes significant restrictions on the handling of such data. In order to address these issues, McMahan *et al.* [3] developed a technique that they termed federated learning (FL), whereby client models train, or update, an instance of a global model using locally captured data and periodically send updated model parameters to a central server for aggregation. By using FL, it is possible to take advantage of numerous distributed datasets while maintaining privacy and reducing communication costs associated with training on a collection of these individual datasets.

Since the seminal work by McMahan *et al.* [3], a significant amount of research has been done to address the numerous challenges associated with implementing an FL framework. This list of challenges includes, but is not limited to, efficiency of communications [4, 5, 6], device heterogeneity [7, 8, 9], statistical heterogeneity [10, 11, 12, 13], and privacy preservation/security [14, 15, 16, 17]. Often, when addressing the aforementioned problems in the FL literature, a deterministic model architecture is assumed [3, 7, 11]. While deterministic deep learning models are capable of achieving high accuracy, they are often uncalibrated [18] (i.e., model-predicted probabilities for each class do not match the empirical frequency for that class) and do not provide access to epistemic (model) uncertainty in prediction. The inability to access epistemic uncertainty is problematic in many remote sensing and other safety-critical applications, where it is important that the underlying model is capable of communicating a measure of epistemic uncertainty in prediction and that the uncertainty be calibrated.

Although the statistics, meteorological, and multi-sensor fusion literature are rich with probabilistic pooling or fusion approaches [19, 20, 21], there does not exist a detailed study of these probabilistic pooling/fusion strategies in the FL setting. Recognizing that there are numerous ways of aggregating, or fusing, probability distributions and that there is no agreed upon technique, Koliander *et al.* [22] provide a comprehensive review of fusion techniques and the motivation for utilizing various fusion techniques and client/site weighting schemes. Utilizing several of the strategies from [22] and additional strategies from [3] and [23], we analyze the effect of fusion techniques in the Bayesian federated learning (BFL) setting, with a focus on the quality of uncertainty. To align with the nomenclature common in FL literature throughout this manuscript, we use the term “aggregate” in place of “fuse” or “pool.”

## 1.2 Contributions

In this paper, we make the following contributions:

1. We re-frame statistical aggregation strategies in the context of FL, specifically for Bayesian deep learning (BDL).
2. We evaluate six aggregation strategies for BDL models in the FL setting on independent and identically distributed (IID) and non-IID partitions of a popular computer vision dataset commonly used to benchmark performance in machine learning (ML) and FL applications. We show that aggregation strategy is a crucial hyperparameter in the design of a BFL algorithm.
3. We evaluate three client weighting strategies in conjunction with each of the six aggregation strategies under evaluation.
4. We examine a popular lightweight Bayesian approximation, Monte Carlo (MC) dropout, in the FL setting and compare its performance to more complex variational inference (VI) models.
5. We evaluate not only the prediction accuracy, but also the calibration and uncertainty (total and decomposed) of both mean-field Gaussian VI and MC dropout VI models used in the FL setting.
6. We share our Flower Federated Learning Framework [24] implementation to facilitate further experimentation with aggregation methods and client weighting techniques on additional datasets.<sup>1</sup>

## 2 Background and Related Work

### 2.1 Federated Learning

In FL, client models train, or update, an instance of a global model using locally captured data and periodically send updated model parameters to a central server for aggregation [3]. Often, this technique is utilized to take advantage of numerous local datasets while maintaining privacy. Additionally, in remote sensing platforms and

<sup>1</sup><https://github.com/meekus-fischer/BayesianFederatedLearning>

other edge devices, FL significantly reduces the communication costs associated with training on these individual datasets. We use the following notation throughout this manuscript:  $k \in \{1, \dots, K\}$  represents the individual clients,  $\mathcal{D}^k = \{(x_1, y_1), \dots, (x_{|\mathcal{D}^k|}, y_{|\mathcal{D}^k|})\}$  represents the local dataset of client  $k$  with  $|\mathcal{D}^k|$  local training examples,  $\mathcal{D}$  comprises the entire training dataset split amongst  $K$  clients,  $\theta_r^k$  is the set of parameters for client  $k$  and FL round  $r$ ,  $\theta_r^g$  is the set of parameters for the global model at round  $r$ ,  $\omega_k$  is the aggregation weight for client  $k$ ,  $B$  is the local minibatch size,  $E$  is the number of local epochs, and  $\eta$  is the learning rate. In general, we can describe the federated optimization problem of  $K$  clients with the following:

$$\min_{\theta \in \mathbb{R}^d} f(\theta^g), \quad \text{where} \quad f(\theta^g) = \sum_{k=1}^K \omega_k f_k(\theta^g). \quad (1)$$

In the ML/FL context,  $f_k(\theta)$  often corresponds to  $\mathcal{L}_k(\mathcal{D}^k, \theta)$ , the local loss of client  $k$  on  $\mathcal{D}^k$  with model parameters  $\theta$ . We place the following constraint on client aggregation weights:  $\sum_{k=1}^K \omega_k = 1$ . In practice, this optimization is done, as described in Alg. 1, over multiple optimization/communication rounds. First, the server initializes the global model (or distributes a pre-trained baseline model) and distributes the model parameters to each of the clients. During each optimization round  $r$ , clients train the global model, using a variant of Stochastic Gradient Descent (SGD), for  $E$  epochs before returning the client parameters to the server. The server then uses an aggregation function (e.g., FedAvg [3]) to combine the model weights and biases of each client into a new global model, and distributes the new global model parameters to each of the clients. This process repeats for  $R$  communication rounds, or until convergence.

---

**Algorithm 1:** Federated Learning.

---

**Server Executes:**

```

initialize  $\theta_0^g$ 
foreach round  $r = 0, 1, \dots, R-1$  do
    foreach client  $k \in \{1, \dots, K\}$  in parallel do
         $\theta_{r+1}^k \leftarrow \text{ClientUpdate}(k, \theta_r^g)$ 
     $\omega = \text{CalculateClientWeights}() \dots$  [Compute  $w_k$  using Eq. (18), (19), (20), or (21)]
     $\theta_{r+1}^g \leftarrow \text{AggregateClients}(\{\theta_{r+1}^1, \dots, \theta_{r+1}^K\}, \omega) \dots$  [Eq. (10), (11), (12), (15), (16), or (17)]
ClientUpdate( $k, \theta_r^g$ ): // Run on client  $k$ 
     $\mathcal{MB} \leftarrow (\text{split } \mathcal{D}^k \text{ into minibatches of size } B)$ 
     $\theta^k \leftarrow \theta_r^g$ 
    foreach local epoch  $i$  from 1 to  $E$  do
        for minibatch  $b \in \mathcal{MB}$  do
             $\theta^k \leftarrow \theta^k - \eta \nabla \ell(\theta^k; b)$ 
    return  $\theta^k$  to the server

```

---

## 2.2 Bayesian Deep Learning

To instill sufficient confidence in the performance, or capability, of ML models for deployment on remote sensing platforms, or safety-critical applications, and to ensure the models are able to adapt to dynamic environments, it is critical that the models are capable of communicating a measure of epistemic uncertainty in prediction [25, 26]. BDL models apply Bayesian methods in order to provide access to the uncertainty measure (epistemic uncertainty), which deterministic ML models are incapable of providing. Instead of utilizing point estimates (deterministic ML), BDL learns a probability distribution over model parameters [27]. BDL has its roots in Bayesian statistics, where inference about model parameters,  $\theta$ , given data,  $\mathcal{D}$ , involves the calculation of the posterior  $p(\theta|\mathcal{D})$ . Placing a prior  $p(\theta)$  on model parameters (e.g., the weights and biases of a BDL architecture) enables the calculation of the posterior distribution of model weights and biases utilizing Bayes' rule:

$$p(\theta|\mathcal{D}) = \frac{p(\mathcal{D}|\theta)p(\theta)}{p(\mathcal{D})}. \quad (2)$$

Ultimately, prediction amounts to calculating

$$p(y^*|x^*, \mathcal{D}) = \int_{\Theta} p(y^*|x^*, \theta) p(\theta|\mathcal{D}) d\theta, \tag{3}$$

where  $x^*$  is the input feature vector,  $y^*$  is a corresponding prediction,  $\Theta$  represents the parameter space of the model, and  $p(y^*|x^*, \mathcal{D})$  is the probability of that prediction given a trained model. Due to the fact that  $p(\mathcal{D})$  in Eq. (2) is not directly accessible, it must be calculated using known quantities.

$$p(\mathcal{D}) = \int_{\Theta} p(\mathcal{D}, \theta) d\theta. \tag{4}$$

High-dimensional integrals, such as the one in Eq. (4), often have no closed form and are computationally intractable [28]. In practice, approximate inference is used. There are many methods for approximate inference; however, two of the most common approaches are Markov Chain Monte Carlo (MCMC) sampling and VI [29]. Although MCMC is often described as the “gold standard” for approximate inference, VI is commonly favored in BDL, due to the increased speed and the ability to scale with large data and large models [30]. There are a number of approaches to implementing VI; two of the most common of implementations—Flipout [31] and Local Reparameterization Trick [32]—use Gaussian distributions and effectively double the number of model parameters. Another common approach, MC dropout, was shown to be an effective Bayesian approximation that does not double the number of model parameters [33]. In many situations, each of these methods has been empirically shown to lead to useful approximation of  $p(\theta|\mathcal{D})$ , providing access to improved uncertainty estimation when compared to the uncertainty provided by deterministic models. In this work, we utilize Flipout VI models and MC dropout models as our BDL models.

The essence of VI is that optimization is used to approximate the true posterior  $p(\theta|\mathcal{D})$  by identifying the closest distribution  $q_{\phi}(\theta)$ , parameterized by  $\phi$ , to the posterior among a family of pre-determined (variational) distributions (commonly a Gaussian). Often, the “closeness” is determined using Kullback-Leibler (KL) divergence, a common information-theoretic measure of similarity between two distributions.

$$KL[q_{\phi}(\theta) || p(\theta|\mathcal{D})] = \int_{\Theta} q_{\phi}(\theta) \log \frac{q_{\phi}(\theta)}{p(\theta|\mathcal{D})} d\theta. \tag{5}$$

The optimization objective for VI then becomes

$$\mathcal{L}_q = \text{KL}[q_{\phi}(\theta) || p(\theta)] - \mathbb{E}_q [\log p(\mathcal{D}|\theta)], \tag{6}$$

where  $\mathbb{E}_q$  represents the expected value under the probability distribution  $q_{\phi}(\theta)$ . In this form, also known as the negative Evidence Lower Bound (ELBO), it becomes clear that the optimization objective is the sum of a data-dependent portion (likelihood cost), and a prior dependent portion (complexity cost) [34].

The quality of the approximation in VI is highly dependent on the choice of the variational distribution family. As mentioned in the previous paragraph, we consider two distinct approaches, a mean-field Gaussian distribution with a Flipout MC estimator of KL-divergence [31] and MC dropout, which uses a Bernoulli distribution over the model weights and biases [33]. In the first, the use of Gaussian distributions, parameterized by the mean and variance of the distribution, doubles the number of parameters in the model architecture, when compared to its deterministic counterpart. The use of the Gaussian distribution results in a more challenging optimization problem relative to MC dropout. In the MC dropout approach, there is no additional increase in the number of model parameters, and minimal changes are required to the model architecture [35, 25, 33]. It is these simplifications that motivate our analysis of the MC dropout model in the FL framework as a lightweight Bayesian approximation.

### 2.3 Uncertainty Quantification and Decomposition

In BDL models used for classification, predictive probability  $p(y = c | x)$  is approximated by using MC integration with  $M$  samples [36]. The mean probability per class  $\bar{p}_c$  is calculated using the prediction probabilities,  $\hat{p}_{c_m}$ , where  $\hat{p}_{c_m} = p(y = c | x, \theta^m)$  and  $\theta^m$  is sampled from an approximation of  $p(\theta|\mathcal{D})$ .

$$\bar{p}_c = \frac{1}{M} \sum_{m=1}^M \hat{p}_{c_m}. \tag{7}$$

The predicted class for each sample is chosen by selecting the class that yields the highest mean probability. In addition to a predicted class, the  $M$  MC samples allow for the calculation of predictive entropy and variance. Predictive entropy has several interpretations; however, in information theory, entropy is interpreted as the amount of information contained in a predictive distribution [28]. Normalized predictive entropy ( $\tilde{H}$ ), for the multi-class classification problem, is given by

$$\tilde{H}_p(y | \mathbf{x}) = - \sum_{c \in C} p(y = c | x) \frac{\log p(y = c | x)}{\log C}, \quad (8)$$

where  $C$  represents all possible classes [37]. Although entropy is commonly used as a measure of aleatoric uncertainty in deterministic and Bayesian deep learning, Depeweg *et al.* [38] interpret entropy as a measure of predictive uncertainty, which could be further broken down into its aleatoric and epistemic uncertainty components. Aleatoric uncertainty is known as data uncertainty and cannot be reduced with an increase in training data. Epistemic uncertainty is known as model uncertainty and can be reduced by increasing the amount of training data [28]. Epistemic uncertainty is not accessible using deterministic models.

For BDL models, variance provides another measure of total uncertainty, which can be broken down into epistemic and aleatoric uncertainty. Kendall *et al.* [26] and Kwon *et al.* [39] separately propose methods for estimating aleatoric and epistemic uncertainty with Kwon *et al.* modifying the approach in [26] to give the following estimator:

$$\underbrace{\frac{1}{M} \sum_{m=1}^M \text{diag}(\hat{p}_m) - \hat{p}_m^{\otimes 2}}_{\text{aleatoric}} + \underbrace{\frac{1}{M} \sum_{m=1}^M (\hat{p}_m - \bar{p}_c)^{\otimes 2}}_{\text{epistemic}}, \quad (9)$$

where  $M$  is the number of MC samples,  $\hat{p}_m$  is a  $c$ -dimensional vector containing the predictive probabilities of each class ( $\hat{p}_{c_m}$ ),  $\text{diag}(\hat{p}_m)$  is a diagonal matrix,  $\hat{p}_m^{\otimes 2} = \hat{p}_m \hat{p}_m^T$ , and  $(\hat{p}_m - \bar{p}_c)^{\otimes 2} = (\hat{p}_m - \bar{p}_c)(\hat{p}_m - \bar{p}_c)^T$ .

## 2.4 Federated Bayesian Learning

In scenarios involving big data with many distributed remote sensing platforms, the need to adapt to dynamic environments, and the need to benefit from the ability to communicate a measure of uncertainty, the application of BDL to FL is a natural one. Several works have applied Bayesian techniques to the FL problem. In [40], the authors apply the Laplace approximation at both the client and server to reduce aggregation errors and regularize, or guide, local model training. Notably, in this work, the authors choose to aggregate client models using a mixture of Gaussians. FedBE [41] constructs a global model by fitting a distribution (Gaussian or Dirichlet) to the client models and sampling from this distribution to arrive at a higher-quality global model. Similarly, FedAG [42] applies uncertainty in the aggregation step by using the client parameters to fit a Gaussian distribution at the server. In [43], the authors present a BFL framework where each client performs approximate Bayesian inference, using MCMC sampling, and distills the clients' posterior distribution into a single deep neural network via knowledge distillation techniques for aggregation at the server. pFedBayes [12] is a personalized FL model that uses VI to learn a personalized local model at each client while learning a shared global model.

With the exception of pFedBayes [12], none of these works employ VI. While pFedBayes [12] utilizes VI, the global model uses a simple averaging method for client parameter aggregation, and no additional methods are discussed, or analyzed. Additionally, in pFedBayes [12], the authors utilize a model with a single variational layer (i.e., with the exception of the output layer, all layers are deterministic). This work is the first time, to our knowledge, that anyone has utilized a fully variational model (i.e., all model layers are variational) to analyze the effects of the choice of aggregation function and client weighting scheme on BDL models in FL.

The use of BDL in FL introduces several unique problems. First, the model weights and biases in a VI model are no longer a point estimate. Each weight and bias is defined by the parameters of a distribution. In the case of a Gaussian, this is the mean and variance of the distribution. In the following sub-sections, we present multiple aggregation strategies for univariate Gaussian distributions and their underlying theory. Next, we discuss the selection of client weights in the aggregation process. Often, the size of the local training dataset is utilized to weight each client. However, this is not the only method, and we present several other weighting schemes for analysis. Finally, in mean-field Gaussian VI we often select priors with a fixed mean of zero and a fixed variance,  $p(\theta) = N(0, \sigma_{prior}^2 I)$ , for the regularization term in

the optimization problem. However, in this work, we pose the question of whether or not to update the prior after each round of optimization. We analyze the effect of updating the prior each round vs. maintaining a fixed prior throughout the training process.

## 2.5 Aggregation Strategies

Although there are a significant number probabilistic aggregation approaches that have been presented in the literature [19, 20, 21], we focus our study on six select strategies from [3, 21, 22, 44, 45] due to their suitability for implementation in the FL construct. In the following sub-sections, we discuss each of these approaches using the univariate Gaussian distribution for each parameter ( $\theta_i$ ), parameterized by its mean ( $\mu_i$ ) and variance ( $\sigma_i^2$ ), as the model distribution. We use univariate Gaussians because of our use of mean-field Gaussian VI, where we assume each parameter is independent. The six approaches are Naive Weighted Averaging (NWA) [3], Weighted Sum of Normal Distributions (WS), Linear Pooling (LP) [22], Conflation/Weighted Conflation (WC) [21, 44], and Distributed Weight Consolidation (DWC) [23]. We use the following notation in our discussion:  $K$  is the set of client models,  $q_k$  is the distribution for client  $k$ ,  $q_g$  is the global (server) distribution, and  $\omega_k$  is the weight of client  $k$  with  $\sum_{k=1}^K \omega_k = 1$ .

### 2.5.1 Naive Weighted Averaging

This aggregation method is similar to the FedAvg algorithm [3] and is simplest of the aggregation techniques. In the case where  $\omega_k = \frac{|\mathcal{D}_k|}{|\mathcal{D}|}$ , NWA is equivalent to FedAvg. Although this method was shown to be effective for aggregating deterministic model weights and biases in [3], independently aggregating the mean and variance parameters in this manner ignores the statistical properties of the Gaussian Distribution. This method is familiar to the statistical literature, however, and is described as Centered Linear Pool (CLP) in [46], and used extensively in [46, 47, 48]. Clements defends the use of this variance calculation in [47] noting that the variance calculated using LP is often inflated by the “disagreement” term (described in Section II.G.3), and the NWA method is equal to the expected variance of a randomly selected client.

$$\mu_{q_g} = \sum_{k=1}^K \omega_k \mu_{q_k}, \quad \sigma_{q_g}^2 = \sum_{k=1}^K \omega_k \sigma_{q_k}^2. \quad (10)$$

Ultimately, this method involves taking the weighted average of each of the clients’ individual model parameters to form the global model without regard for what each of the parameters represents.

### 2.5.2 Weighted Sum of Normal Distributions

If the mean and variance of each model parameter are considered as part of a univariate Gaussian distribution, instead of being considered individually as in NWA, it is possible to take the weighted average of each of the client Gaussian distributions. This strategy assumes the weights of each client are mutually independent.

$$\mu_{q_g} = \sum_{k=1}^K \omega_k \mu_{q_k}, \quad \sigma_{q_g}^2 = \sum_{k=1}^K \omega_k^2 \sigma_{q_k}^2. \quad (11)$$

The resultant Gaussian distribution in WS has the same mean as in NWA, but the variance parameter differs. Because the  $\omega$  parameter falls in the range of  $[0, 1]$ , and we square each client’s weight parameter  $\omega_k$  in WS, the variance parameter in WS will always be less than or equal to the variance parameter in NWA.

### 2.5.3 Linear Pooling

The LP technique is studied extensively in the forecasting literature [49, 46, 48, 50, 51, 52] and is connected to model averaging and multiple model adaptive estimation (MMAE) [53], as described by Koliander *et al.* in [22]. To derive the LP operator for univariate Gaussian random variables, we define each client distribution as  $q_k(\theta) = \mathcal{N}(\theta; \mu_{q_k}, \sigma_{q_k})$  where  $\mu_{q_k} = \mathbb{E}_{q_k}[\theta]$  and  $\sigma_{q_k}^2 = \mathbb{E}_{q_k}[\theta - \mu_{q_k}]^2$ . LP is then defined as the linear combination of each of the client distributions:

$$q_g(\theta) = \sum_{k=1}^K \omega_k \mathcal{N}(\theta; \mu_{q_k}, \sigma_{q_k}). \quad (12)$$

The global mean is then defined by  $\mu_{q_g} = \mathbb{E}_{q_g}[\theta]$ , which is just the weighted average of the client means ( $\mu_{q_k}$ ):

$$\mu_{q_g} = \sum_{k=1}^K \omega_k \mu_{q_k}. \quad (13)$$

The global variance can similarly be defined as  $\sigma_{q_g}^2 = \mathbb{E}_{q_g}[\theta - \mu_{q_g}]^2$ , which is broken down by Lahiri *et al.* [54] into two components. The first component is the weighted average variance of each client  $\sigma_{q_k}^2$ . The second component is the “disagreement” component of the global variance and captures the discrepancy between clients.

$$\begin{aligned} \sigma_{q_g}^2 &= \underbrace{\sum_{k=1}^K \omega_k \sigma_{q_k}^2}_{\text{avg client var}} + \underbrace{\sum_{k=1}^K \omega_k (\mu_{q_k} - \mu_{q_g})^2}_{\text{disagreement term}} \\ &= \sum_{k=1}^K \omega_k (\sigma_k^2 + (\mu_k - \mu_{q_g})^2). \end{aligned} \quad (14)$$

In [46], the authors show that LP imposes an upward bias on the global variance resulting in under-confident predictions. We briefly mentioned one of the ways in which researchers have dealt with this upward bias in the NWA subsection. CLP, which is equivalent to NWA, is a variant of LP which ignores the disagreement term in the LP variance calculation and reduces this upward bias.

#### 2.5.4 Conflation and Weighted Conflation

The Conflation and WC methods [21, 44] are the normalized product of client distributions and are closely related to Log-Linear Pooling (LLP) [22]. LLP is a weighted geometric average of client distributions and is so named because it is a linear function of client distributions in the log-domain [22]. When combining Gaussian distributions, LLP differs from WC only in the numerator of the global variance term, with LLP replacing  $\omega_{max}$  with a value of 1. As shown in [21, 44], Conflation/WC has several desirable properties. These properties include:

- Conflation/WC is commutative, associative, and iterative.
- The resulting distribution of the Conflation/WC of Gaussian distributions is a Gaussian.
- The result of the Conflation/WC of Gaussian distributions matches the result of the weighted-least-squares method.
- Conflation/WC minimizes the loss of Shannon information as a result of the consolidation of multiple Gaussian distributions into a single Gaussian distribution.
- Conflation/WC is the best linear unbiased estimate.
- Conflation/WC yields a maximum likelihood estimator.

We provide the formulas for both Conflation, Eq. (15), and WC, Eq. (16), below.

$$\mu_{q_g} = \frac{\sum_{k=1}^K \frac{\mu_{q_k}}{\sigma_{q_k}^2}}{\sum_{k=1}^K \frac{1}{\sigma_{q_k}^2}}, \quad \sigma_{q_g}^2 = \frac{1}{\sum_{k=1}^K \frac{1}{\sigma_{q_k}^2}}. \quad (15)$$

Readers familiar with the Inverse Variance Weighting (IV) technique [45] may notice that the Conflation formula, Eq. (15), is identical to the formula for IV. IV is a well-known method for combining random variables in such a way as to minimize the variance of the resulting distribution.

$$\mu_{q_g} = \frac{\sum_{k=1}^K \frac{\omega_k \mu_{q_k}}{\sigma_{q_k}^2}}{\sum_{k=1}^K \frac{\omega_k}{\sigma_{q_k}^2}}, \quad \sigma_{q_g}^2 = \frac{\omega_{max}}{\sum_{k=1}^K \frac{\omega_k}{\sigma_{q_k}^2}}. \quad (16)$$

Notably, WC produces a Gaussian distribution with a mean value which is proportional to the client weights, inversely proportional to client variances, and has a variance which is never greater than the variance of the client with the greatest weight.

### 2.5.5 Distributed Weight Consolidation

DWC was introduced by McClure *et al.* [23] as a continual learning technique to combine or consolidate the model weights and biases of multiple Bayesian neural networks (BNNs) trained on independent datasets. This method builds on the concept of Variational Continual Learning [55] and Bayesian Incremental Learning [56]. However, both of these methods require that the underlying models be trained sequentially. In DWC, multiple disparate models (clients) can be trained independently, and their weights and biases can be consolidated into a single network (global model), similar to the FL setting. DWC is related to the Supra-Bayesian framework described in [22], which involves the selection of a prior distribution,  $p(\theta)$ , and the update of the prior using a Bayesian update rule. In DWC, we are using the global model,  $q_o(\theta)$ , as the prior,  $p(\theta)$ , and applying the same Bayesian update rule. In Eq. (17), we provide the formulas for the global mean and variance, the derivation of which can be found in [23].

$$\mu_{q_g} = \frac{\sum_{k=1}^K \frac{\mu_{q_k}}{\sigma_{q_k}^2} - \sum_{k=1}^{K-1} \frac{\mu_{q_o}}{\sigma_{q_o}^2}}{\sum_{k=1}^K \frac{1}{\sigma_{q_k}^2} - \sum_{k=1}^{K-1} \frac{1}{\sigma_{q_o}^2}}, \quad \sigma_{q_g}^2 = \frac{1}{\sum_{k=1}^K \frac{1}{\sigma_{q_k}^2} - \sum_{k=1}^{K-1} \frac{1}{\sigma_{q_o}^2}}. \quad (17)$$

where  $\mu_{q_o}$  and  $\sigma_{q_o}^2$  correspond to the global mean and variance from the previous round, respectively. It should be noted that DWC was designed to start with a base model trained on some initial dataset, and not a random initialization. Additionally, in the DWC setting, each ‘‘client’’ trains asynchronously on their local dataset before aggregating client parameters. This is the first time that this method has been applied to and analyzed in the BFL setting.

## 2.6 Determining Weight Parameters

In the seminal work on FL, McMahan *et al.* [3] weighted client updates based on the size of each client’s local dataset relative to the datasets of all other clients. Although this method is common in FL, there have been several works [57, 22] which explore various techniques for weighting clients to achieve varying objectives (robustness against outliers, reducing communications, training efficiency, etc.). We treat the client weighting scheme as a hyperparameter and analyze the results (with a focus on uncertainty) of using four different techniques for selecting client weights. Notably, the implementation of several of these methods require that the underlying models be Bayesian. As such, we only apply each weighting technique to models for which it is applicable.

### 2.6.1 Equal Weight

The first, and simplest, method is to give equal weight to each client in the update process using Eq. (18). In addition to its simplicity, it does not require any a priori knowledge of the client datasets. As a result, it is completely independent of the amount of training data, or the quality of training data, at each client site, and is not resistant to outliers or extreme updates. This method is applicable to both deterministic and probabilistic models.

$$\omega_k = \frac{1}{K}. \quad (18)$$

### 2.6.2 Local Train Dataset Size

This method was introduced in [3], and is widely used in the FL literature. In order to apply this weighting scheme, the server either needs to have a priori knowledge of the size of the client datasets, or the client needs to communicate the size of their training dataset with the model update. When the data is distributed evenly amongst clients, this method, Eq. (19), is equivalent to Equal Weight. This method is applicable to both deterministic and probabilistic models. Since each of our dataset partitions results in clients having an equal amount of data, this method is equivalent to Equal Weight.

$$\omega_k = \frac{|\mathcal{D}_k|}{|\mathcal{D}|}. \quad (19)$$



### 2.6.3 Maximum Discrepancy Weighting

Koliander *et al.* described maximum discrepancy weighting in [22]. This technique involves treating the client weights as a measure of distance. In Eq. (20), we use Kullback Leibler Divergence. However, other measures of distance or divergence could be used. By computing client weights in this manner, the server places higher importance on model weights and biases that are not extreme (relative to the other clients). The gamma value ( $\gamma_k$ ) and omega value ( $\omega_k$ ) in Eq. (20) are the un-normalized and normalized weights of each client, respectively. This method is only applicable to probabilistic models. However, a similar technique could be used in deterministic models using the L2 norm, or another measure of distance. We only apply this technique to the probabilistic (VI) models.

$$\gamma_k = \max_{j \in \{1, \dots, K\}} \frac{1}{\text{KL}[q_k || q_j]}, \quad \omega_k = \frac{\gamma_k}{\sum_{j=1}^K \gamma_j}. \quad (20)$$

### 2.6.4 Distance to a Fixed Point

This method is similar to maximum discrepancy weighting in that it also treats client weights as a measure of distance. Instead of calculating the divergences between the distributions of the model weights and biases for individual clients, we use the divergence between the distributions of the model weights and biases for individual clients and the global model from the previous round. In effect, this places a greater importance on clients that do not diverge significantly from the current global model. Similar to maximum discrepancy weighting, the gamma value ( $\gamma_k$ ) and omega value ( $\omega_k$ ) in Eq. (21) are the un-normalized and normalized weights of each client, respectively. Again, this method is only applicable to probabilistic models; however, a similar technique could be used in deterministic models using the L2 norm, or another measure of distance. We only apply this technique to the probabilistic (VI) models.

$$\gamma_k = \frac{1}{\text{KL}[q_g || q_k]}, \quad \omega_k = \frac{\gamma_k}{\sum_{j=1}^K \gamma_j}. \quad (21)$$

## 3 Experiments

### 3.1 Datasets

We utilize the CIFAR-10 [58] image classification dataset to benchmark our models and model parameter aggregation rules. The CIFAR-10 dataset consists of 50,000 training images and 10,000 test images of size 32x32x3 pixels, which belong to one of 10 classes. Similar to [3, 10, 59], we adopt both an IID and non-IID partitioning strategy. In both strategies, we partition the training dataset amongst 10 clients. For the IID strategy, we assign each client a uniform distribution over the 10 classes. For the non-IID strategy, we follow the strategy introduced by Li *et al.* in [59] and adopt both a quantity-based label imbalance and a distribution-based label imbalance. In the quantity-based label imbalance scenario, we first sort the data by class and divide the data into 20 partitions of size 2,500, and randomly assign each client two partitions from different classes (i.e., each client training dataset contains examples from two classes with 2,500 examples of each class). In the distribution-based label imbalance scenario, each client is allocated a proportion of the samples of each label according to the Dirichlet distribution, which is parameterized by  $\alpha$  [60]. In our experiment, we use  $\alpha$  parameters of 0.5 and 5.0 to simulate different levels of class imbalance across client training datasets.

### 3.2 Architecture

We utilize the Flower Federated Learning Framework [24] to implement the FL setup. In order to conduct a fair comparison of performance across model configurations, we utilize the ResNet-20 [61] architecture in a deterministic, MC dropout [33], and Flipout [31] (VI) configuration, as shown in Fig. 1. Notably, when trained on a centralized training dataset, all variants of the ResNet-20 model used in this paper achieved comparable performance to the benchmark performance reported by He *et al.* [61] on the CIFAR-10 dataset, see Table 1. The models were coded using Tensorflow v2.9 and Tensorflow Probability v0.16 [62] and all experiments were performed on NVIDIA RTX 8000 graphics processing units.

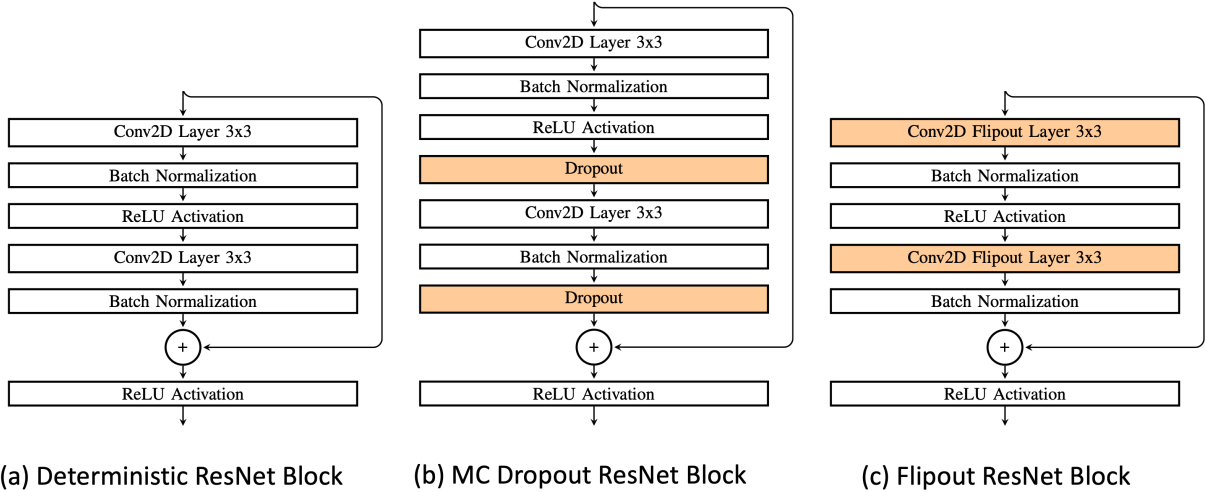


Figure 1: ResNet Model Block Structure. (a) depicts the structure of a ResNet block in the deterministic configuration. (b) depicts the structure of the same ResNet block in the MC dropout configuration with the addition of a dropout layer after each convolutional and linear layer. These dropout layers are enabled during the inference phase. (c) depicts the ResNet block in the Flipout configuration. Each convolutional and linear layer is replaced by the Tensorflow Probability implementation of the corresponding Flipout Layer. Changes from the deterministic configuration are highlighted in orange.

Table 1: ResNet-20 Centralized Training Results

Model	Accuracy
Deterministic	90.14
MC Dropout	90.91
Flipout	90.42

### 3.3 General Experiment Setup and Evaluation Metrics

For all experiments, we utilize  $K = 10$  clients,  $B = 32$  local minibatch size, and  $\eta = .001$  initial local learning rate with an exponential schedule that reduces the learning rate by a factor of .04 every round after a silent period of 50 aggregation rounds. Additionally, we use a dropout rate of 0.2 for MC dropout models and our Flipout models use  $p(\theta) = N(0, 100I)$ .

We present the results of each experiment using accuracy and negative log likelihood (NLL). NLL is equivalent to the KL Divergence between a model’s predicted distribution and a one-hot encoded true distribution [28], with a lower NLL corresponding to a better representation. In terms of calibration, Filos *et al.* [36] demonstrated that if a model’s performance increases as the number of discarded high-uncertainty predictions increases, the model is well-calibrated. As a result, we utilize accuracy vs. data retained curves to assess the calibration of models based on normalized predictive entropy, aleatoric uncertainty, and epistemic uncertainty.

### 3.4 Evaluation of Aggregation Methods - 1 Local Epoch

In this experiment, we evaluate each of the proposed aggregation strategies with  $E = 1$  local epochs. Each simulation is run three times for 400 rounds, and the results, shown in Table 2, are averaged across experiments.

In terms of accuracy and NLL, no aggregation strategy outperforms other aggregation strategies on all data distributions. Notably, NWA and LP do not perform as well as WS, WC, and conflation, which all perform similarly to the deterministic model baseline (NWA). LP performs especially poorly on all data distributions.

Uncertainty calibration plots are depicted in Fig. 2. When looking at the bulk uncertainty metric (normalized entropy), in the IID and non-IID Dirichlet (0.5 and 5.0) cases, all of the global models display a calibrated uncertainty. Even though the global models are calibrated, the models trained using WS, WC, and conflation appear to be better calibrated than the models trained using LP and NWA (i.e., test accuracy increases more rapidly as the most uncertain samples are discarded from the test data). By breaking down the bulk uncertainty into its epistemic and aleatoric components, the

performance difference is amplified. Specifically, when filtering based on epistemic uncertainty, models trained using WS, WC, and conflation perform much better than those trained using LP and NWA. In the non-IID 2-Class case, the relationships between aggregation strategies is similar. However, not all the global models have a calibrated epistemic uncertainty component.

In Fig. 3, we plot learning curve comparisons (test set accuracy vs federation round) for each of the data distributions. Again, models trained using WS, WC, and conflation exhibit similar behavior. The models trained using each of these aggregation methods converge much faster than the LP and NWA strategies.

Table 2: Simulation Results - Site Epochs ( $E = 1$ )

Model	Agg. Fn.	Client Weighting	IID		Non-IID 2-Class		Non-IID Dir ( $\alpha = 0.5$ )		Non-IID Dir ( $\alpha = 5.0$ )	
			Accuracy	NLL	Accuracy	NLL	Accuracy	NLL	Accuracy	NLL
Deterministic	NWA	Train Size	87.66 ± 0.001	0.370 ± 0.005	51.45 ± 0.020	1.55 ± 0.040	83.45 ± 0.003	0.485 ± 0.008	85.78 ± 0.003	0.435 ± 0.001
MC Dropout	NWA	Train Size	89.19 ± 0.001	0.330 ± 0.006	47.20 ± 0.020	1.65 ± 0.020	85.52 ± 0.002	0.431 ± 0.004	87.45 ± 0.002	0.373 ± 0.005
		Distance	81.67 ± 0.002	0.576 ± 0.004	43.04 ± 0.025	1.68 ± 0.006	74.77 ± 0.008	0.721 ± 0.015	79.89 ± 0.002	0.62 ± 0.005
Flipout (VI)	NWA	Max Disc	81.28 ± 0.001	0.581 ± 0.002	47.81 ± 0.024	1.65 ± 0.013	75.45 ± 0.009	0.722 ± 0.005	80.06 ± 0.003	0.608 ± 0.012
		Distance	81.76 ± 0.003	0.576 ± 0.007	40.00 ± 0.030	1.80 ± 0.036	75.92 ± 0.011	0.717 ± 0.003	80.04 ± 0.001	0.614 ± 0.002
		Distance	87.41 ± 0.002	0.388 ± 0.006	53.52 ± 0.056	1.41 ± 0.076	83.74 ± 0.002	0.508 ± 0.014	85.17 ± 0.004	0.465 ± 0.01
	WS	Max Disc	87.81 ± 0.004	0.377 ± 0.004	47.72 ± 0.049	1.49 ± 0.048	84.17 ± 0.004	0.487 ± 0.008	84.90 ± 0.002	0.476 ± 0.001
		Distance	87.55 ± 0.003	0.391 ± 0.004	51.84 ± 0.014	1.47 ± 0.021	83.23 ± 0.003	0.51 ± 0.005	85.07 ± 0.002	0.464 ± 0.005
		Distance	77.21 ± 0.004	0.683 ± 0.007	35.50 ± 0.048	1.85 ± 0.046	67.67 ± 0.008	0.925 ± 0.02	74.7 ± 0.007	0.744 ± 0.016
LP	Max Disc	77.35 ± 0.004	0.681 ± 0.012	37.86 ± 0.018	1.79 ± 0.014	69.35 ± 0.009	0.895 ± 0.017	76.01 ± 0.011	0.717 ± 0.023	
	Distance	77.69 ± 0.002	0.674 ± 0.005	32.48 ± 0.064	1.90 ± 0.085	68.47 ± 0.015	0.914 ± 0.034	75.94 ± 0.005	0.721 ± 0.009	
	Distance	87.95 ± 0.001	0.377 ± 0.006	53.00 ± 0.052	1.44 ± 0.096	83.18 ± 0.004	0.510 ± 0.009	85.09 ± 0.003	0.478 ± 0.001	
WC	Max Disc	87.81 ± 0.002	0.384 ± 0.004	50.71 ± 0.025	1.49 ± 0.044	83.70 ± 0.002	0.514 ± 0.004	84.86 ± 0.002	0.470 ± 0.005	
	Distance	87.52 ± 0.002	0.389 ± 0.002	46.41 ± 0.037	1.52 ± 0.037	83.17 ± 0.001	0.514 ± 0.006	85.23 ± 0.002	0.464 ± 0.006	
	Distance	87.42 ± 0.001	0.385 ± 0.003	53.09 ± 0.008	1.46 ± 0.027	83.18 ± 0.001	0.502 ± 0.008	84.94 ± 0.005	0.471 ± 0.008	
Conflation	N/A									

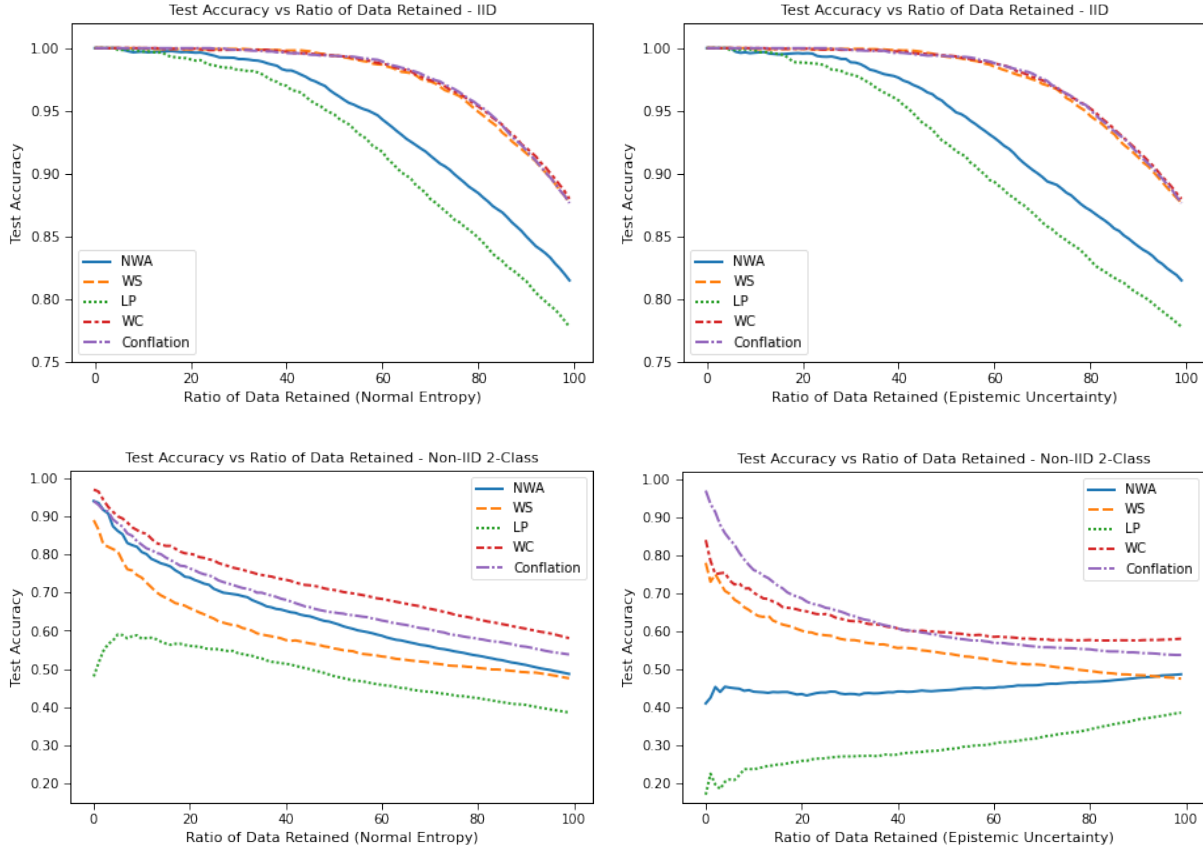


Figure 2: Uncertainty calibration plots for  $E = 1$ . VI aggregation method comparison plot of test set accuracy vs. ratio of data retained for IID and non-IID 2-class data distributions. Non-IID Dirichlet distribution plots show trends and relationships that mirror IID distribution results. Normalized entropy and epistemic uncertainty plots are shown, aleatoric uncertainty plots show trends and relationships that mirror normalized entropy.

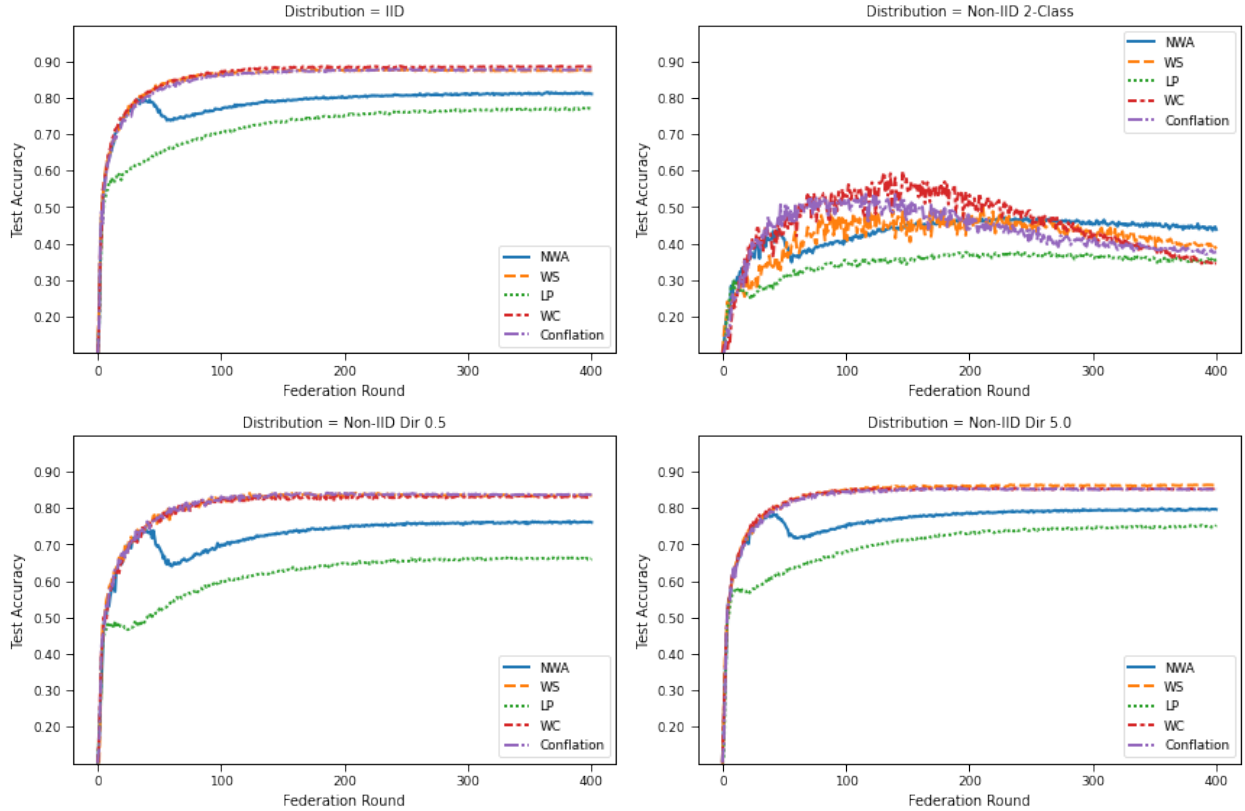


Figure 3: Learning curve plots for  $E = 1$ . Plot of test set accuracy vs. federation round for VI aggregation methods for each data distribution.

### 3.5 Evaluation of Aggregation Methods - 5 Local Epochs

Next, we increase the amount of client computation and evaluate each of the proposed aggregation strategies with  $E = 5$  local epochs. Each simulation is run three times for 200 rounds, and the results, shown in Table 3, are averaged across experiments.

The results, depicted in Table 3, show much more parity between aggregation strategies in terms of accuracy and NLL. In fact, models trained using the NWA strategy perform as well as, or better, than the other aggregation strategies across the board. When compared to the  $E = 1$  experiment results (Table 2), models employing WS, WC, and conflation show minimal improvement when client computation is increased. In some cases (WC/conflation - non-IID 2-class), the models trained using  $E = 5$  actually perform worse. Notably, none of the VI aggregation methods perform as well as the deterministic baseline on the IID or non-IID Dirichlet data distributions. However, all of them significantly improve on the deterministic baseline in the non-IID 2-class case.

Similar to the accuracy and NLL results, the calibration differences across aggregation strategies are drastically reduced in the IID and non-IID Dirichlet cases. However, as is the case in the  $E = 1$  experiments, NWA and LP do not display a calibrated epistemic uncertainty component. The learning curve comparison plots in Fig. 5 display the same relationships as their  $E = 1$  counterparts in Fig. 3.

### 3.6 Evaluation of Aggregation Methods - DWC and Model Pre-training

The results of the DWC experiments are presented separately due to significant differences in the training setup required by the DWC aggregation strategy. In Table 4, we present DWC results with and without global model pre-training. For comparison, we employ the same pre-training strategy using the WS aggregation method. Each of the DWC and model pre-training experiments is run three times for a single federation round, where each client trains for 400 local epochs. Before distributing the global model to each client, the server pre-trains the global model on 10% of the CIFAR-10

Table 3: Simulation Results - Site Epochs ( $E = 5$ )

Model	Agg. Fn.	Client Weighting	IID		Non-IID 2-Class		Non-IID Dir ( $\alpha = 0.5$ )		Non-IID Dir ( $\alpha = 5.0$ )	
			Accuracy	NLL	Accuracy	NLL	Accuracy	NLL	Accuracy	NLL
Deterministic	NWA	Train Size	90.74 ± 0.003	0.371 ± 0.009	48.50 ± 0.040	1.56 ± 0.060	87.33 ± 0.002	0.456 ± 0.008	89.06 ± 0.002	0.456 ± 0.008
MC Dropout	NWA	Train Size	91.16 ± 0.002	0.264 ± 0.003	44.90 ± 0.040	1.58 ± 0.030	87.91 ± 0.001	0.357 ± 0.002	89.53 ± 0.002	0.316 ± 0.001
Flipout (VI)	NWA	Train Size	88.76 ± 0.002	0.334 ± 0.005	56.36 ± 0.017	1.55 ± 0.021	85.26 ± 0.001	0.439 ± 0.001	87.46 ± 0.001	0.380 ± 0.004
		Max Disc	88.87 ± 0.001	0.336 ± 0.002	55.91 ± 0.061	1.55 ± 0.083	85.43 ± 0.001	0.435 ± 0.002	87.30 ± 0.003	0.380 ± 0.002
		Distance	88.98 ± .003	0.332 ± 0.004	45.60 ± 0.129	1.59 ± 0.098	85.35 ± 0.003	0.436 ± 0.008	87.38 ± 0.001	0.377 ± 0.001
	WS	Train Size	88.37 ± 0.004	0.446 ± 0.008	56.96 ± 0.004	1.36 ± 0.015	84.53 ± 0.002	0.585 ± 0.004	85.51 ± 0.002	0.545 ± 0.002
		Max Disc	88.23 ± 0.005	0.429 ± 0.002	49.84 ± 0.036	1.42 ± 0.012	84.68 ± 0.004	0.587 ± 0.005	84.92 ± 0.009	0.554 ± 0.006
		Distance	88.34 ± 0.003	0.444 ± 0.003	48.49 ± 0.021	1.42 ± 0.017	84.91 ± 0.004	0.581 ± 0.005	85.75 ± 0.007	0.545 ± 0.014
	LP	Train Size	88.05 ± 0.002	0.358 ± 0.002	55.41 ± 0.023	1.60 ± 0.040	83.59 ± 0.001	0.478 ± 0.006	86.36 ± 0.001	0.408 ± 0.003
		Max Disc	88.19 ± 0.001	0.356 ± 0.001	48.87 ± 0.031	1.65 ± 0.041	84.00 ± 0.003	0.472 ± 0.008	86.62 ± 0.002	0.404 ± 0.004
		Distance	87.91 ± 0.001	0.363 ± 0.004	41.95 ± 0.050	1.65 ± 0.049	84.03 ± 0.001	0.471 ± 0.004	86.47 ± 0.001	0.408 ± 0.004
	WC	Train Size	88.21 ± 0.002	0.443 ± 0.002	52.23 ± 0.027	1.41 ± 0.040	84.49 ± 0.004	0.583 ± 0.006	86.01 ± 0.006	0.542 ± 0.014
		Max Disc	88.34 ± 0.002	0.430 ± 0.007	49.21 ± 0.051	1.49 ± 0.059	83.52 ± 0.002	0.589 ± 0.012	84.47 ± 0.014	0.548 ± 0.012
		Distance	88.28 ± 0.005	0.437 ± 0.012	48.25 ± 0.026	1.44 ± 0.043	85.17 ± 0.005	0.574 ± 0.009	85.37 ± 0.007	0.578 ± 0.006
Conflation	N/A		88.16 ± 0.008	0.444 ± 0.006	52.47 ± 0.028	1.39 ± 0.031	84.86 ± 0.003	0.586 ± 0.015	85.59 ± 0.006	0.550 ± 0.003

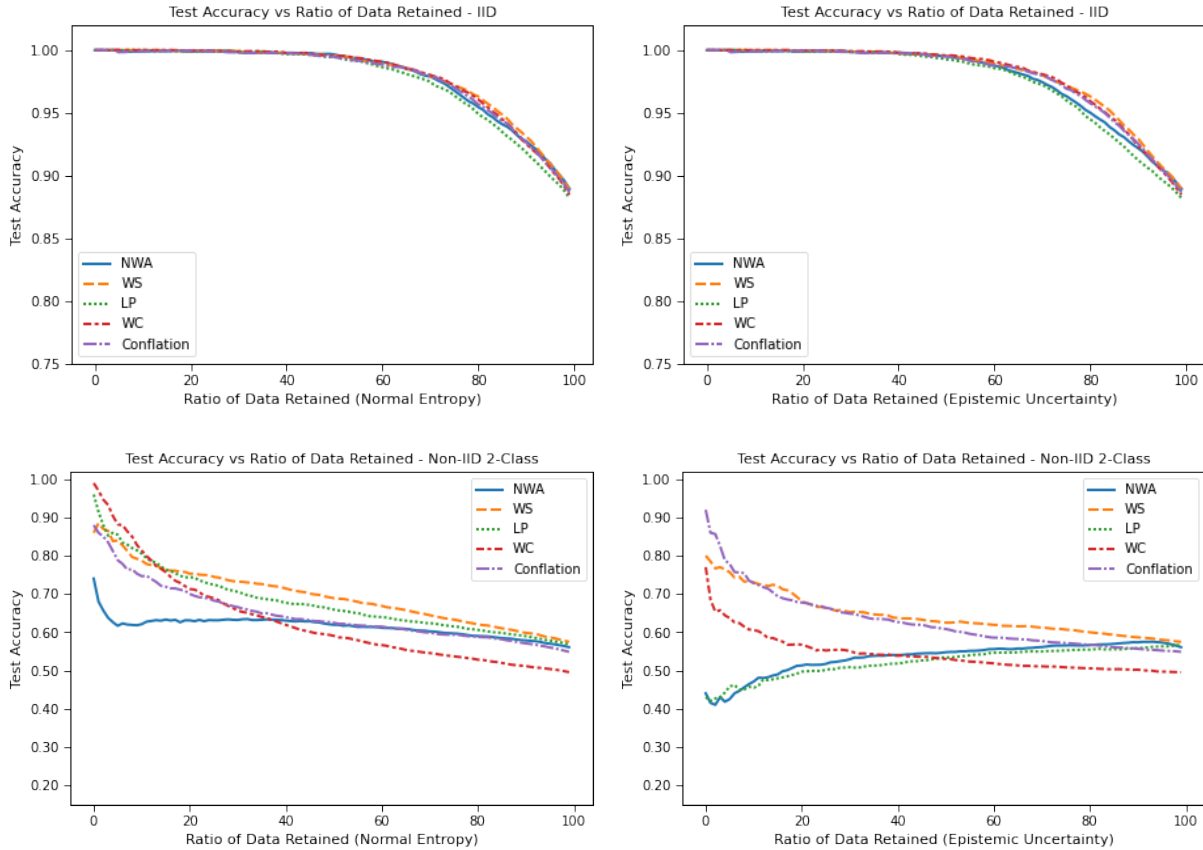


Figure 4: Uncertainty calibration plots for  $E = 5$ . VI aggregation method comparison plot of test set accuracy vs. ratio of data retained for IID and non-IID 2-class data distributions. Non-IID Dirichlet distribution plots show trends and relationships that mirror IID distribution results. Normalized entropy and epistemic uncertainty plots are shown, aleatoric uncertainty plots show trends and relationships that mirror normalized entropy.

dataset for a maximum of 100 local epochs. To avoid overfitting in our global model pre-training, we employ an early stopping strategy which monitors validation accuracy with a patience of 10 epochs.

In Table 4, the first row holds the results for DWC without pre-training the global model. In this case, DWC does not hold up as a viable aggregation method. One of the potential explanations for the poor performance of DWC in this setup, is the use of a randomly initialized model as the initial global model. This is due to fact that the global model is heavily weighted in DWC. As a result, we experimented with pre-training the global model on a small subset of the overall training dataset. This setup more closely resembles the experimental setup in [23]. Additionally, this is a likely

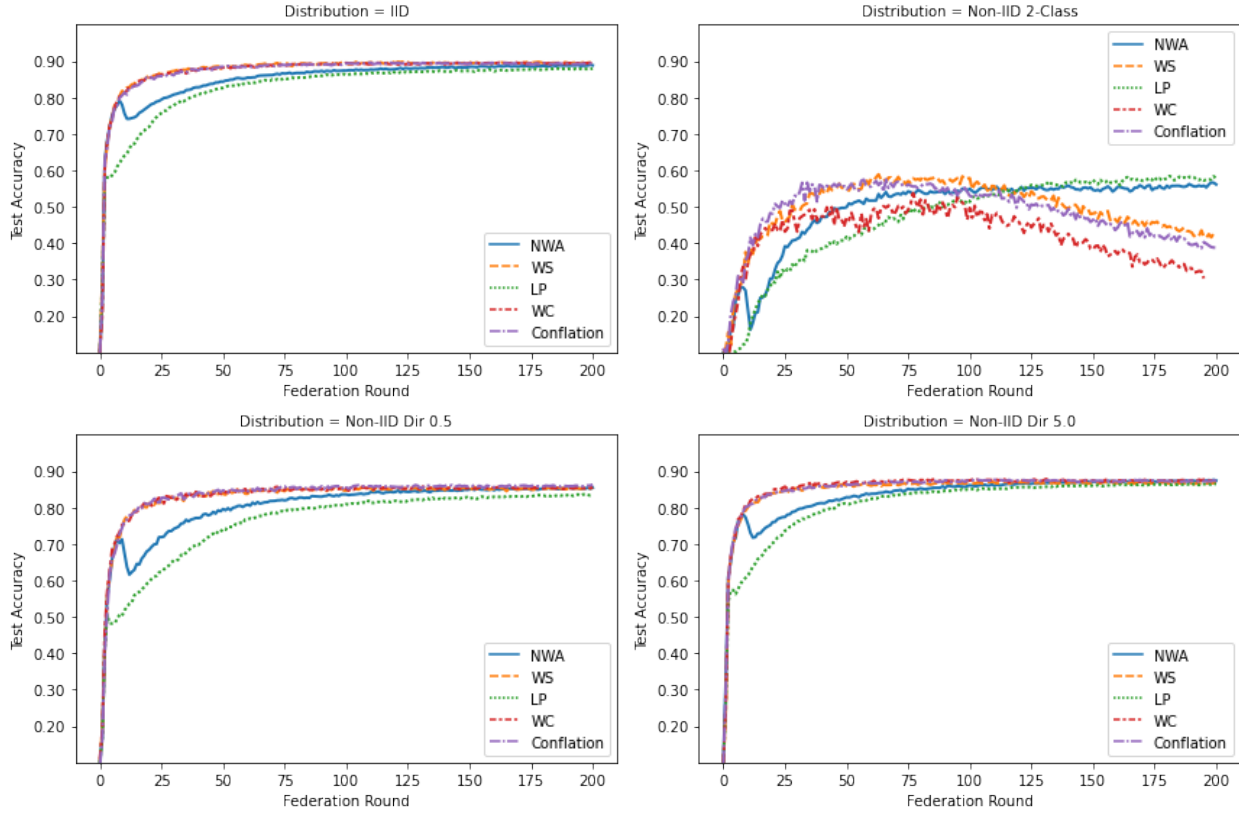


Figure 5: Learning curve plots for  $E = 5$ . Plot of test set accuracy vs. federation round for VI aggregation methods for each data distribution.

scenario for a network of distributed sensors where a model is pre-trained on a centralized dataset and deployed on a group of sensors for collaborative learning.

In terms of accuracy and NLL, our pre-training setup does not perform comparably to the  $E = 1$  or  $E = 5$  experiments in the IID and Non-IID Dirichlet cases. On the other hand, in the non-IID 2-class case, the models that were pre-trained perform exceedingly well. In addition to a significant improvement in accuracy and NLL, the uncertainty calibration plots in Fig. 6 display well-calibrated bulk (normalized entropy) and decomposed (aleatoric and epistemic) uncertainty components.

Table 4: Simulation Results - DWC

Model	Agg. Fn.	Pre-train	IID		Non-IID 2-Class		Non-IID Dir ( $\alpha = 0.5$ )		Non-IID Dir ( $\alpha = 5.0$ )	
			Accuracy	NLL	Accuracy	NLL	Accuracy	NLL	Accuracy	NLL
Flipout	DWC	No	34.95 $\pm$ 1.230	1.73 $\pm$ 0.031	11.64 $\pm$ 1.73	2.69 $\pm$ 0.220	17.25 $\pm$ 3.14	2.440 $\pm$ 0.210	31.83 $\pm$ 1.05	1.801 $\pm$ 0.029
Flipout	DWC	Yes	71.42 $\pm$ 0.270	0.83 $\pm$ 0.007	66.35 $\pm$ 1.53	0.97 $\pm$ 0.038	68.81 $\pm$ 0.42	0.918 $\pm$ 0.007	65.87 $\pm$ 1.36	0.972 $\pm$ 0.026
Flipout	WS	Yes	72.70 $\pm$ 0.008	0.80 $\pm$ 0.017	64.63 $\pm$ 1.02	1.01 $\pm$ 0.051	62.65 $\pm$ 0.02	1.061 $\pm$ 0.061	68.18 $\pm$ 0.02	0.913 $\pm$ 0.051

### 3.7 Updating the Prior Every Federation Round

In this experiment, we assess the effect of updating the prior after every federation round. Each of these experiments are run twice on the IID data partition, and the results are averaged across experiments. The results in Table 5 show a precipitous drop in accuracy and NLL when compared to the results in Tables 2 and 3, demonstrating that updating the prior every federation round is not an effective strategy.

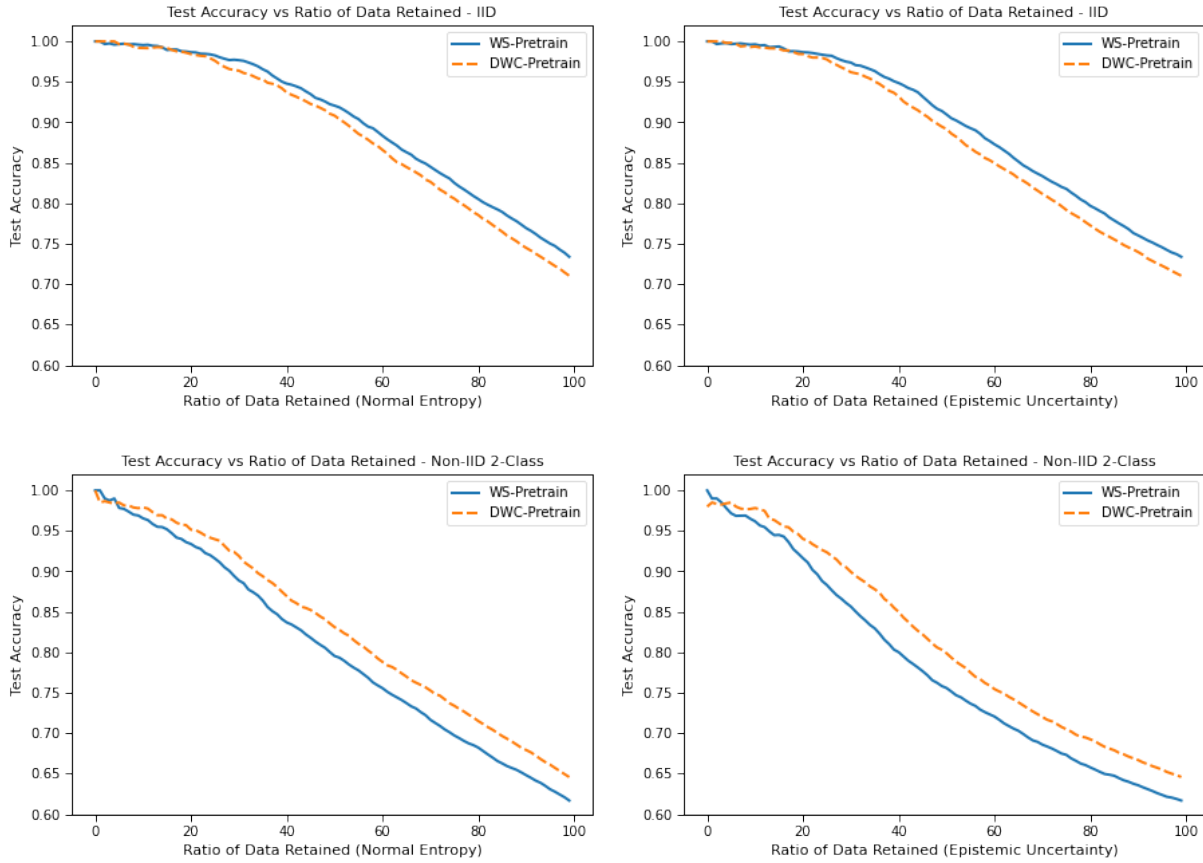


Figure 6: Uncertainty calibration plots for global model pre-training experiments. DWC and WS aggregation method comparison plot of test set accuracy vs. ratio of data retained for IID and non-IID 2-class data distributions. Non-IID Dirichlet distribution plots show trends and relationships that mirror IID distribution results. Normalized entropy and epistemic uncertainty plots are shown, aleatoric uncertainty plots show trends and relationships that mirror normalized entropy.

Table 5: Simulation Results - Prior Updated Every Federation Round ( $E = 1$ )

		IID		
Model	Agg. Fn.	Client Weighting	Accuracy	NLL
Flipout (VI)	NWA	Train Size	41.84 ± .59	1.55 ± .009
	WS	Train Size	43.54 ± .54	1.53 ± .017
	LP	Train Size	46.14 ± .50	1.46 ± .011
	WC	Train Size	44.23 ± .52	1.51 ± .002
	Conflation	N/A	42.62 ± .58	1.56 ± .007

### 3.8 Client Weighting Strategies

Results of the  $E = 1$  and  $E = 5$  experiments with different client weighting strategies are depicted in Tables 2 and 3. These experiments were conducted in conjunction with the  $E = 1$  and  $E = 5$  experiments, and utilized the same setup. Unfortunately, this experiment was inconclusive, and the results did not elucidate the importance of the different client weighting techniques.

### 3.9 MC Dropout as a Lightweight Alternative to Mean-field Gaussian VI

The MC dropout experiments were conducted in conjunction with the  $E = 1$  and  $E = 5$  experiments and the setup is the same. Accuracy and NLL results are presented in Tables 2 and 3.

For both  $E = 1$  and  $E = 5$ , in terms of accuracy/NLL, the MC dropout models using NWA perform similarly to the deterministic baseline. In the IID and non-IID Dirichlet cases, the MC dropout models outperform all the VI aggregation methods. On the other hand, in the non-IID 2-class case, the MC dropout model does not perform nearly as well as the top-performing VI aggregation methods.

In Fig. 7, we present uncertainty calibration comparison plots for  $E = 1$ . Like the previous uncertainty calibration plots, the non-IID Dirichlet plots depict the same trends and relationships as the IID plots and are not shown. The  $E = 5$  calibration plots also follow similar relationships and trends to the  $E = 1$  plots and are not shown. In both cases, the models trained on IID and non-IID Dirichlet data distributions appear to be well-calibrated. In contrast, in the non-IID 2-class case, the MC dropout models show poor calibration of the epistemic uncertainty.

Figures 8 and 9 depict the learning curve comparisons for  $E = 1$  and  $E = 5$ . Similar to the calibration plots, WS is used as a reference for comparison. For  $E = 1$ , the MC dropout models converge at a marginally slower rate. In the non-IID 2-class case for  $E = 5$ , shown in Fig. 9, the MC dropout model converges at a significantly slower rate than the mean-field Gaussian VI model trained using WS.

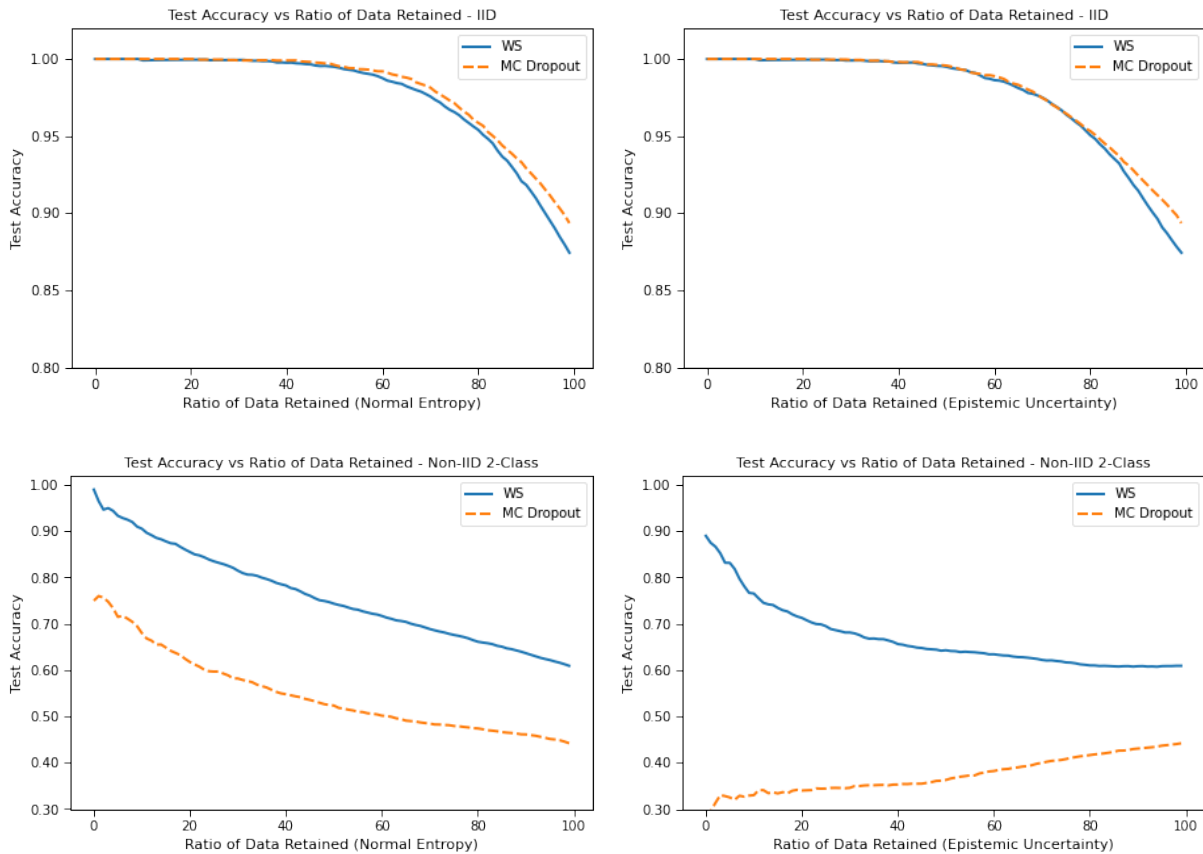


Figure 7: Uncertainty calibration plots for MC dropout experiments ( $E = 1$ ). MC dropout (NWA) and VI (WS) aggregation method comparison plot of test set accuracy vs. ratio of data retained for IID and non-IID 2-class data distributions. Non-IID Dirichlet distribution plots show trends and relationships that mirror IID distribution results. Normalized entropy and epistemic uncertainty plots are shown, aleatoric uncertainty plots show trends and relationships that mirror normalized entropy.

## 4 Discussion

In our evaluation of six different aggregation methods, and three client weighting schemes, we demonstrated that the results vary based on the training data distribution and number of local training epochs per federation round. We showed that the selection of the aggregation method is a critical hyperparameter, with downstream effects on model performance (accuracy), calibration, and training time, which must be selected based on the machine learning model



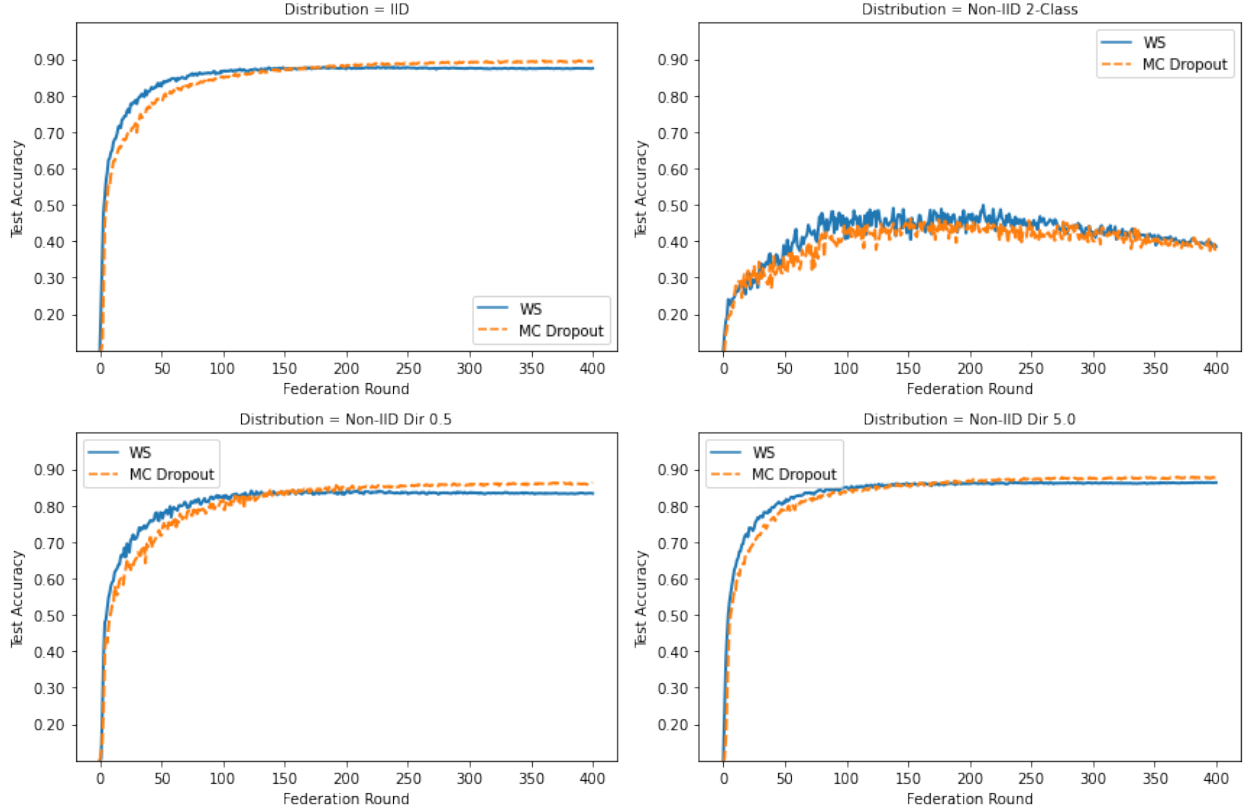


Figure 8: Learning curve plots for MC dropout experiments ( $E = 1$ ). Plot of test set accuracy vs. federation round for MC dropout (NWA) and VI (WS) aggregation methods for each data distribution.

type, dataset, and other hyperparameters. Notably, we established that often these aggregation strategies can be placed into two groups, with each group exhibiting similar performance (accuracy/NLL), calibration, and convergence rate. The first group consists of WS, WC, and conflation. The second group consists of NWA and LP. Models employing the aggregation strategies in the first group tend to exhibit relatively high accuracy, low NLL, and rapid convergence with a single local epoch of training during each federation round. These models are also better calibrated than their counterparts from the second group, which require five local epochs of training per federation round to reach the same performance level. These relationships may facilitate a targeted hyperparameter search. Specifically, the similarities amongst strategies in each group may allow the testing of a single strategy from each group to narrow the search.

Although our experiments on client weighting techniques were not fruitful, we believe that this may be due to the CIFAR-10 dataset and the model we selected. In FL implementations with more complex architectures and complex, real-world, datasets, where distributions are highly non-IID, these weighting techniques may help to smooth training and reduce the effects of a non-representative client or an adversary attempting to disrupt the training process. Further experimentation with larger and more complex models and datasets is necessary to validate these beliefs.

The DWC algorithm required some significant adjustments to our experimental setup; however, it drove us to experiment with pre-training. In many remote sensing tasks, like visual target recognition or passive sonar target classification [63], this setup is likely. Prior to deployment on a remote sensing platform, the model needs to be trained and evaluated on a representative dataset until it demonstrates an acceptable level of performance. The random initialization is not realistic in these remote sensing applications. Once the model is deployed on a group of sensors, it can be fine-tuned using FL in a setup that mirrors our experimental setup. In this application, DWC is a viable solution and displays comparable performance to WS.

The cost of deploying VI models to remote sensing platforms and training those models, in many cases, is prohibitive. MC dropout is a lightweight alternative to mean-field Gaussian VI which, prior to this work, has not been directly compared to VI in the FL environment. In our experiments, we showed that in the IID and non-IID Dirichlet cases, MC dropout performs on par with one of the top performing VI aggregation methods (WS). In fact, in terms of accuracy and NLL, the MC dropout models outperform the mean-field Gaussian VI models. Although the mean-field Gaussian

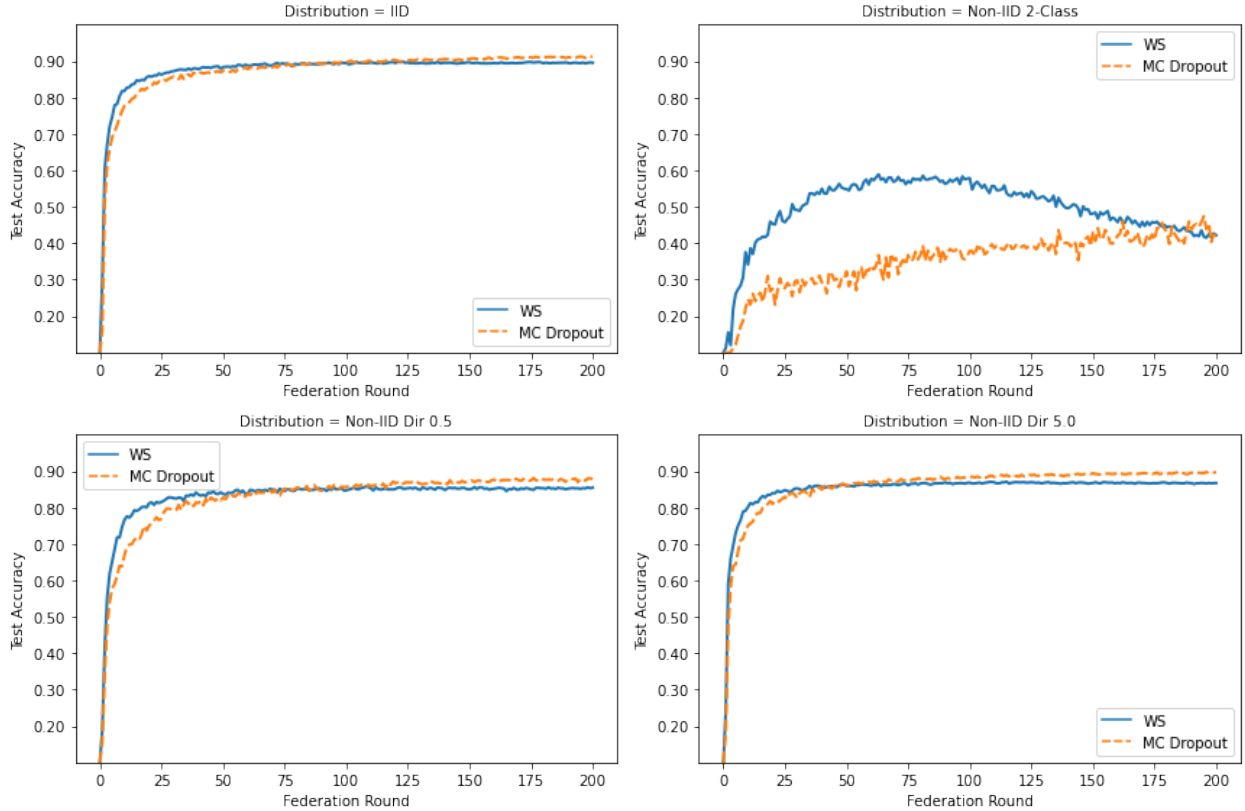


Figure 9: Learning curve plots for MC dropout experiments ( $E = 5$ ). Plot of test set accuracy vs. federation round for MC dropout (NWA) and VI (WS) aggregation methods for each data distribution.

VI models tended to converge faster, the MC dropout models have half the number of parameters, which require fewer client resources and lower communication requirements between client and server. The non-IID 2-class data distribution case was the exception: the MC dropout models converged slower, showed a reduction in accuracy, and displayed poor calibration. In some cases, the use of an MC dropout model utilizing the NWA aggregation strategy may be an acceptable lightweight alternative to mean-field Gaussian VI models employing one of the aggregation strategies discussed in this manuscript.

## 5 Conclusion and Future Work

In remote sensing and safety-critical applications, the ability of a model to communicate a measure of epistemic uncertainty is essential. BDL models are capable of communicating a measure of epistemic uncertainty while simultaneously delivering competitive prediction accuracy when compared to their deterministic counterparts. However, to fully realize the benefits of BDL in the FL setting, it is important to understand the downstream effects of the selected model aggregation method. In this manuscript, we used four different partitions of the CIFAR-10 dataset and a fully variational ResNet-20 architecture to analyze six BFL model aggregation methods for mean-field Gaussian VI models. This is the first time, to our knowledge, that a fully variational architecture (i.e., all model layers are variational) has been utilized in this type of analysis. Additionally, when trained on a centralized dataset, each of the variants of our ResNet-20 architecture achieved comparable performance to the benchmark performance reported by He *et al.* [61], see Table 1. As such, we were able to compare our FL results to an important ML benchmark and provide a more detailed look at uncertainty. Ultimately, we identified the aggregation method as a critical hyperparameter in the development of a BFL strategy, and we showed that, in certain applications, MC dropout is an acceptable lightweight alternative to mean-field Gaussian VI. In both cases (mean-field Gaussian VI and MC dropout), our global models (Table 3,  $E = 5$ ) achieved test set accuracy within  $\pm 2 - 3\%$  of the centralized benchmark.

## 6 Disclaimer

The views and conclusions contained herein are those of the authors and should not be interpreted as necessarily representing the official policies or endorsements, either expressed or implied, of the U.S. Government. The U.S. Government is authorized to reproduce and distribute reprints for Government purposes notwithstanding any copyright annotations thereon.

## References

- [1] Patricia Mabry, “Making sense of the data explosion: The promise of systems science,” *American Journal of Preventive Medicine*, vol. 40, pp. S159–61, May 2011.
- [2] Paul Voigt and Axel von dem Bussche, *The EU General Data Protection Regulation (GDPR): A Practical Guide*, Springer Publishing Company, Incorporated, 1st edition, 2017.
- [3] Brendan McMahan, Eider Moore, Daniel Ramage, Seth Hampson, and Blaise Aguera y Arcas, “Communication-efficient learning of deep networks from decentralized data,” in *Proceedings of the 20th International Conference on Artificial Intelligence and Statistics*. Apr. 2017, vol. 54 of *Proceedings of Machine Learning Research*, pp. 1273–1282, PMLR.
- [4] Jakub Konečný, H. Brendan McMahan, Felix X. Yu, Peter Richtárik, Ananda Theertha Suresh, and Dave Bacon, “Federated learning: Strategies for improving communication efficiency,” *arXiv preprint arXiv:1610.05492*, 2016.
- [5] Hangyu Zhu and Yaochu Jin, “Multi-objective evolutionary federated learning,” *IEEE Transactions on Neural Networks and Learning Systems*, vol. 31, no. 4, pp. 1310–1322, 2019.
- [6] Felix Sattler, Simon Wiedemann, Klaus-Robert Müller, and Wojciech Samek, “Robust and communication-efficient federated learning from non-I.I.D. data,” *IEEE Transactions on Neural Networks and Learning Systems*, vol. 31, no. 9, pp. 3400–3413, 2020.
- [7] Tian Li, Anit Kumar Sahu, Manzil Zaheer, Maziar Sanjabi, Ameet Talwalkar, and Virginia Smith, “Federated optimization in heterogeneous networks,” in *Proceedings of Machine Learning and Systems*, 2020, vol. 2, pp. 429–450.
- [8] Xiaohui Xu, Sijing Duan, Jinrui Zhang, Yunzhen Luo, and Deyu Zhang, “Optimizing federated learning on device heterogeneity with a sampling strategy,” in *2021 IEEE/ACM 29th International Symposium on Quality of Service (IWQoS)*, 2021, pp. 1–10.
- [9] Yassine Laguel, Krishna Pillutla, Jérôme Malick, and Zaid Harchaoui, “A superquantile approach to federated learning with heterogeneous devices,” in *2021 55th Annual Conference on Information Sciences and Systems (CISS)*, 2021, pp. 1–6.
- [10] Yue Zhao, Meng Li, Liangzhen Lai, Naveen Suda, Damon Civin, and Vikas Chandra, “Federated learning with non-IID data,” *arXiv preprint arXiv:1806.00582*, 2018.
- [11] Canh T. Dinh, Nguyen Tran, and Josh Nguyen, “Personalized federated learning with Moreau envelopes,” in *Advances in Neural Information Processing Systems*, 2020, vol. 33, pp. 21394–21405.
- [12] Xu Zhang, Yinchuan Li, Wenpeng Li, Kaiyang Guo, and Yunfeng Shao, “Personalized federated learning via variational Bayesian inference,” in *Proceedings of the 39th International Conference on Machine Learning*. Jul. 2022, vol. 162 of *Proceedings of Machine Learning Research*, pp. 26293–26310, PMLR.
- [13] Alireza Fallah, Aryan Mokhtari, and Asuman Ozdaglar, “Personalized federated learning with theoretical guarantees: A model-agnostic meta-learning approach,” in *Advances in Neural Information Processing Systems*, 2020, vol. 33, pp. 3557–3568.
- [14] Keith Bonawitz, Vladimir Ivanov, Ben Kreuter, Antonio Marcedone, H. Brendan McMahan, Sarvar Patel, Daniel Ramage, Aaron Segal, and Karn Seth, “Practical secure aggregation for privacy-preserving machine learning,” in *Proceedings of the 2017 ACM SIGSAC Conference on Computer and Communications Security*, 2017, CCS ’17.
- [15] Robin C. Geyer, Tassilo Klein, and Moin Nabi, “Differentially private federated learning: A client level perspective,” *arXiv preprint arXiv:1712.07557*, 2017.
- [16] Abhishek Bhowmick, John C. Duchi, Julien Freudiger, Gaurav Kapoor, and Ryan Rogers, “Protection against reconstruction and its applications in private federated learning,” *arXiv preprint arXiv:1812.00984*, 2018.
- [17] Liping Li, Wei Xu, Tianyi Chen, Georgios B. Giannakis, and Qing Ling, “RSA: Byzantine-robust stochastic aggregation methods for distributed learning from heterogeneous datasets,” *Proceedings of the AAAI Conference on Artificial Intelligence*, vol. 33, no. 01, pp. 1544–1551, Jul. 2019.

- [18] Chuan Guo, Geoff Pleiss, Yu Sun, and Kilian Q. Weinberger, “On calibration of modern neural networks,” in *Proceedings of the 34th International Conference on Machine Learning*. Aug. 2017, vol. 70 of *Proceedings of Machine Learning Research*, pp. 1321–1330, PMLR.
- [19] Zhansheng Duan, X. Rong Li, and U. D. Hanebeck, “Multi-sensor distributed estimation fusion using minimum distance sum,” in *17th International Conference on Information Fusion (FUSION)*, 2014, pp. 1–8.
- [20] Christian Genest and James V. Zidek, “Combining probability distributions: A critique and an annotated bibliography,” *Statistical Science*, vol. 1, no. 1, pp. 114 – 135, 1986.
- [21] Theodore Hill, “Conflations of probability distributions,” *Transactions of the American Mathematical Society*, vol. 363, Aug. 2008.
- [22] Gunther Koliander, Yousef El-Laham, Petar Djuric, and Franz Hlawatsch, “Fusion of probability density functions,” *Proceedings of the IEEE*, vol. 110, pp. 404–453, 04 2022.
- [23] Patrick McClure, Charles Y Zheng, Jakub Kaczmazzyk, John Rogers-Lee, Satra Ghosh, Dylan Nielson, Peter A Bandettini, and Francisco Pereira, “Distributed weight consolidation: A brain segmentation case study,” in *Advances in Neural Information Processing Systems*, 2018, vol. 31.
- [24] Daniel J Beutel, Taner Topal, Akhil Mathur, Xinchu Qiu, Titouan Parcollet, and Nicholas D Lane, “Flower: A friendly federated learning research framework,” *arXiv preprint arXiv:2007.14390*, 2020.
- [25] Yarin Gal, *Uncertainty in Deep Learning*, Ph.D. thesis, Dept. of Engineering, University of Cambridge, Cambridge, England, 2016.
- [26] Alex Kendall and Yarin Gal, “What uncertainties do we need in Bayesian deep learning for computer vision?,” in *Advances in Neural Information Processing Systems*, I. Guyon, U. V. Luxburg, S. Bengio, H. Wallach, R. Fergus, S. Vishwanathan, and R. Garnett, Eds., 2017, vol. 30.
- [27] David M Blei, Alp Kucukelbir, and Jon D McAuliffe, “Variational inference: A review for statisticians,” *Journal of the American Statistical Association*, vol. 112, no. 518, pp. 859–877, 2017.
- [28] Oliver Durr, Beate Sick, and Elvis Murina, *Probabilistic Deep Learning With Python, Keras and TensorFlow Probability*, chapter 8, Manning Publications Co., 2020.
- [29] Christopher M Bishop, *Pattern Recognition and Machine Learning*, Springer, New York, NY, USA, 2006.
- [30] Matthew D. Hoffman, David M. Blei, Chong Wang, and John Paisley, “Stochastic variational inference,” *Journal of Machine Learning Research*, vol. 14, no. 4, pp. 1303–1347, 2013.
- [31] Yeming Wen, Paul Vicol, Jimmy Ba, Dustin Tran, and Roger Grosse, “Flipout: Efficient pseudo-independent weight perturbations on mini-batches,” in *International Conference on Learning Representations*, 2018.
- [32] Durk P Kingma, Tim Salimans, and Max Welling, “Variational dropout and the local reparameterization trick,” in *Advances in Neural Information Processing Systems*, 2015, vol. 28.
- [33] Yarin Gal and Zoubin Ghahramani, “Dropout as a Bayesian approximation: Representing model uncertainty in deep learning,” in *Proceedings of The 33rd International Conference on Machine Learning*. 20–22 Jun 2016, vol. 48 of *Proceedings of Machine Learning Research*, pp. 1050–1059, PMLR.
- [34] Charles Blundell, Julien Cornebise, Koray Kavukcuoglu, and Daan Wierstra, “Weight uncertainty in neural networks,” in *Proceedings of the 32nd International Conference on Machine Learning*. Jul. 2015, vol. 37 of *Proceedings of Machine Learning Research*, pp. 1613–1622, PMLR.
- [35] Yarin Gal, Riashat Islam, and Zoubin Ghahramani, “Deep Bayesian active learning with image data,” in *Proceedings of the 34th International Conference on Machine Learning*. Aug. 2017, vol. 70 of *Proceedings of Machine Learning Research*, pp. 1183–1192, PMLR.
- [36] Angelos Filos, Sebastian Farquhar, Aidan N Gomez, Tim GJ Rudner, Zachary Kenton, Lewis Smith, Milad Alizadeh, Arnoud de Kroon, and Yarin Gal, “A systematic comparison of Bayesian deep learning robustness in diabetic retinopathy tasks,” 2019.
- [37] Laurence A. F. Park and Simeon Simoff, “Using entropy as a measure of acceptance for multi-label classification,” in *Advances in Intelligent Data Analysis XIV*. 2015, pp. 217–228, Springer International Publishing.
- [38] Stefan Depeweg, Jose-Miguel Hernandez-Lobato, Finale Doshi-Velez, and Steffen Udfluft, “Decomposition of uncertainty in Bayesian deep learning for efficient and risk-sensitive learning,” in *Proceedings of the 35th International Conference on Machine Learning*. Jul. 2018, vol. 80 of *Proceedings of Machine Learning Research*, pp. 1184–1193, PMLR.

- [39] Yongchan Kwon, Joong-Ho Won, Beom Joon Kim, and Myunghee Cho Paik, “Uncertainty quantification using Bayesian neural networks in classification: Application to biomedical image segmentation,” *Computational Statistics & Data Analysis*, vol. 142, 2020.
- [40] L. Liu, X. Jiang, F. Zheng, H. Chen, G. Qi, H. Huang, and L. Shao, “A Bayesian federated learning framework with online Laplace approximation,” *IEEE Transactions on Pattern Analysis & Machine Intelligence*, vol. 46, no. 01, pp. 1–16, Jan. 2024.
- [41] Hong-You Chen and Wei-Lun Chao, “FedBE: Making Bayesian model ensemble applicable to federated learning,” in *International Conference on Learning Representations*, 2021.
- [42] Adam Thor Thorgeirsson and Frank Gauterin, “Probabilistic predictions with federated learning,” *Entropy*, vol. 23, no. 1, Dec. 2020.
- [43] Shrey Bhatt, Aishwarya Gupta, and Piyush Rai, “Bayesian federated learning via predictive distribution distillation,” 2022.
- [44] Theodore P. Hill and Jack Miller, “How to combine independent data sets for the same quantity,” *Chaos: An Interdisciplinary Journal of Nonlinear Science*, vol. 21, no. 3, Sep. 2011.
- [45] William G. Cochran and Sarah Porter Carroll, “A sampling investigation of the efficiency of weighting inversely as the estimated variance,” *Biometrics*, vol. 9, no. 4, pp. 447–459, 1953.
- [46] Malte Knüppel and Fabian Krüger, “Forecast uncertainty, disagreement, and the linear pool,” *Journal of Applied Econometrics*, vol. 37, no. 1, pp. 23–41, 2022.
- [47] Michael P. Clements, “Are macroeconomic density forecasts informative?,” *International Journal of Forecasting*, vol. 34, no. 2, pp. 181–198, 2018.
- [48] Victor Zarnowitz and Louis A. Lambros, “Consensus and uncertainty in economic prediction,” *Journal of Political Economy*, vol. 95, no. 3, pp. 591–621, 1987.
- [49] M. Stone, “The opinion pool,” *The Annals of Mathematical Statistics*, vol. 32, no. 4, pp. 1339 – 1342, 1961.
- [50] Michael P. Clements, “Forecast uncertainty—ex ante and ex post: U.S. inflation and output growth,” *Journal of Business & Economic Statistics*, vol. 32, no. 2, pp. 206–216, 2014.
- [51] Kajal Lahiri and Xuguang Sheng, “Measuring forecast uncertainty by disagreement: The missing link,” *Journal of Applied Econometrics*, vol. 25, Feb. 2008.
- [52] Christian Genest and Kevin McConway, “Allocating the weights in the linear opinion pool,” *Journal of Forecasting*, vol. 9, pp. 53–73, 1990.
- [53] P.D. Hanlon and P.S. Maybeck, “Multiple-model adaptive estimation using a residual correlation Kalman filter bank,” *IEEE Transactions on Aerospace and Electronic Systems*, vol. 36, no. 2, pp. 393–406, 2000.
- [54] Kajal Lahiri, Christie Teigland, and Mark Zaporowski, “Interest rates and the subjective probability distribution of inflation forecasts,” *Journal of Money, Credit and Banking*, vol. 20, no. 2, pp. 233–248, 1988.
- [55] Cuong V. Nguyen, Yingzhen Li, Thang D. Bui, and Richard E. Turner, “Variational continual learning,” in *International Conference on Learning Representations*, 2018.
- [56] Max Kochurov, Timur Garipov, Dmitry Podoprikin, Dmitry Molchanov, Arsenii Ashukha, and Dmitry Vetrov, “Bayesian incremental learning for deep neural networks,” 2018.
- [57] Jonatan Reyes, Lisa Di-Jorio, Cécile Low-Kam, and Marta Kersten-Oertel, “Precision-weighted federated learning,” *arXiv preprint arXiv:2107.09627*, 2021.
- [58] Alex Krizhevsky, “Learning multiple layers of features from tiny images,” M.s. thesis, University of Toronto, Toronto, Ontario, Canada, 2009.
- [59] Qinbin Li, Yiqun Diao, Quan Chen, and Bingsheng He, “Federated learning on non-IID data silos: An experimental study,” in *2022 IEEE 38th International Conference on Data Engineering (ICDE)*, 2022, pp. 965–978.
- [60] Tzu-Ming Harry Hsu, Hang Qi, and Matthew Brown, “Measuring the effects of non-identical data distribution for federated visual classification,” *arXiv preprint arXiv:1909.06335*, 2019.
- [61] Kaiming He, Xiangyu Zhang, Shaoqing Ren, and Jian Sun, “Deep residual learning for image recognition,” in *2016 IEEE Conference on Computer Vision and Pattern Recognition (CVPR)*, 2016, pp. 770–778.
- [62] Martín Abadi, Ashish Agarwal, Paul Barham, Eugene Brevdo, Zhifeng Chen, Craig Citro, Greg S. Corrado, Andy Davis, Jeffrey Dean, Matthieu Devin, Sanjay Ghemawat, Ian Goodfellow, Andrew Harp, Geoffrey Irving, Michael Isard, Yangqing Jia, Rafal Jozefowicz, Lukasz Kaiser, Manjunath Kudlur, Josh Levenberg, Dandelion Mané, Rajat Monga, Sherry Moore, Derek Murray, Chris Olah, Mike Schuster, Jonathon Shlens, Benoit Steiner, Ilya Sutskever,

- Kunal Talwar, Paul Tucker, Vincent Vanhoucke, Vijay Vasudevan, Fernanda Viégas, Oriol Vinyals, Pete Warden, Martin Wattenberg, Martin Wicke, Yuan Yu, and Xiaoqiang Zheng, “TensorFlow: Large-scale machine learning on heterogeneous distributed systems,” 2015.
- [63] John Fischer, Marko Orescanin, Paul Leary, and Kevin B. Smith, “Active Bayesian deep learning with vector sensor for passive sonar sensing of the ocean,” *IEEE Journal of Oceanic Engineering*, vol. 48, no. 3, pp. 837–852, 2023.